Available online at www.sciencedirect.com
ScienceDirect
Journal of Sound and Vibration 305 (2007) 172–193
JOURNAL OF SOUND AND VIBRATION
www.elsevier.com/locate/jsvi

Coupled vibrations of a rotor with slant crack

Ashish K. Darpe

Department of Mechanical Engineering, Indian Institute of Technology, Hauz Khas, New Delhi 110016, India

Received 8 January 2007; accepted 22 March 2007
Available online 30 May 2007

Abstract

A finite element model of a rotor with slant crack is presented. Based on fracture mechanics, a new flexibility matrix for the slant crack is derived that accounts for the additional stress intensity factors due to orientation of the crack compared to the transverse crack. Comparison between rotor with slant and transverse crack is made with regard to the stiffness coefficients and coupled vibration response characteristics. Compared to transverse crack, the stiffness matrix for slant crack is more populated with additional cross coupled coefficients. The influence of angle of orientation of the slant crack on the stiffness values is also investigated. Although the torsional stiffness is almost the same for both types of cracks, the larger cross-coupled stiffness values for slant crack leads to stronger cross-coupling in the bending–torsional–longitudinal vibrations compared to the transverse crack. Response-dependent nonlinear breathing crack model is used to evaluate response to unbalance and torsional excitation of the cracked rotor. The comparative study with transverse crack rotor is carried out to explore distinctive features in their response and suggest methodologies to diagnose them.

1. Introduction

An ever-increasing quest for more power has led to severely stressed rotors, particularly in power generation sector. Turborotors of most power generation industry are either close to the end of their design life or have outlived the design life. Due to economic considerations and the possibility of using sophisticated health monitoring techniques available these days, these rotors are still operated. With several locations where stresses (both mechanical and thermal) can increase despite best design practices, fatigue cracks are always a possibility in such rotors. If undetected early, such cracks can pose a potential source of catastrophic failures. Several researchers have therefore conducted extensive investigations on the response of cracked rotor over the last three decades.

An in-depth literature review of dynamics of cracked rotors was published by Wauer [1] and later a more exhaustive state of the art review on rotors as well as structures was published by Dimarogonas [2]. While several authors [3–5] mainly focussed their work on unbalance lateral vibration response of the cracked rotor, others [6–10] investigated and proposed new methods of crack detection based on coupling of vibration due to the presence of crack in a rotor. Although the high level of bending stresses are encountered in the rotors used in industry, torsional stresses are also encountered in many applications and even in case of rotors with no

E-mail address: akdarpe@mech.iitd.ernet.in.

0022-460X/$ - see front matter © 2007 Elsevier Ltd. All rights reserved.
doi:10.1016/j.jsv.2007.03.079

apparent torsional loading. Short circuiting at the terminals, faulty synchronisation, line switching and load rejection, etc., are some of the causes that lead to abnormal torque in generator and turbine shafts. Torsional loads can lead to the development of cracks in rotors that are not transverse but oblique to the shaft axis.

Relatively less work is reported on oblique (slant) crack in the rotor during the past 3 decades of research on cracked rotors. Ichimonji and Watanabe [11] investigated response of the rotor with slant crack. They modelled the rotor with a differential equation with parametric excitation assuming the slant crack opens and closes synchronously with torsional excitation frequency. However, only qualitative study was carried out. Later Ichimonji et al. [12] presented quantitative analysis using three-dimensional finite element (3D FE) model. Sekhar and Prasad [13] also presented FE analysis by deriving first the flexibility matrix on similar lines as the work of Papadopoulos and Dimarogonas [14] and then made use of this matrix in the FE model of the rotor with slant crack. The breathing of the crack is modelled by assuming the stiffness variation of the rotor by a truncated cosine series. The stiffness matrix is assumed to vary synchronously with frequency of torsional excitation. The torsional vibration response is then analysed under unbalance and torsional excitation. Based on the same FE modelling Prabhakar et al. [15] investigated transient response of the rotor with slant crack.

The vibration-based detection of crack in a rotor is based on changes in the dynamic behaviour of the rotor due to the presence of crack. A fatigue transverse surface crack in the rotor brings about change in the stiffness of the rotor that gives qualitative changes in the vibration response of the rotor. Although the change in stiffness is quantitatively small (4–10% depending upon the depth of the crack) it is sufficient to bring about distinguishing changes in the frequency content of the vibration response. Apart from the drop in stiffness, the cracked rotor exhibits one per revolution periodical stiffness variation, which is due to the gradual opening and closing of the crack, known as crack breathing. It is this stiffness variation and the nonlinearity associated with the breathing of the crack that generates higher harmonic components in the response of a rotor with constant radial load such as gravity. It is therefore essential to model the stiffness variation correctly before analysing the vibration response. In contrast to transverse crack, in case of slant crack the crack orientation is expected to yield different way of crack breathing, particularly with torsional excitation.

This paper deals with an FE modeling of a rotor with slant/oblique crack. A more refined crack FE representing slant crack is proposed. The model considers appropriate coupling mechanisms some of which are distinctly different for slant crack compared to the transverse crack due to the geometry and orientation of the slant crack. In addition, a more accurate breathing mechanism is considered that is nonlinear and response dependent and is expected to reveal correct stiffness variation of the slant crack under both excitations—only unbalance and unbalance with torsional excitation. Based on fracture mechanics concepts the flexibility matrix is first derived. The matrix differs from the one derived by Sekhar and Prasad [13]. They have derived a flexibility matrix that has the same cross-coupling terms as the transverse crack although with different magnitude. However, due to the orientation of the slant crack with shaft axis, it is expected that additional stress intensity factors (SIFs) could be introduced. For example, the torsional load would not only introduce sliding and tearing mode SIF but will also be responsible to the opening mode SIF. These aspects have not been considered in Ref. [13]. In this paper, comparative study of response of rotors with slant and transverse crack is carried out and vibration response features specific to each type of crack are identified.

2. Finite element representation of rotor segment with slant crack

The rotor-bearing system is modelled using Timoshenko beam element with 6° of freedom per node. However to account for the presence of slant crack, the rotor segment with crack is modelled separately. The mass matrix is assumed unchanged for the cracked rotor segment and only the stiffness matrix is modified. In this section, flexibility matrix for the rotor FE with a slant crack is derived.

Consider a rotor segment of radius R and length l with a slant crack having a depth of a oriented at an angle of θ relative to the axis of the shaft. The element is loaded with shear forces P_2, P_3 and P_8, P_9, bending moments P_4, P_5 and P_{11}, P_{12}, axial forces P_1 and P_7 and torsional moments P_4 and P_{10} (Fig. 1). Thus all the six degrees of freedom per node is considered here. The centre of the crack is situated at a distance x from the left end of the element as shown in the figure.

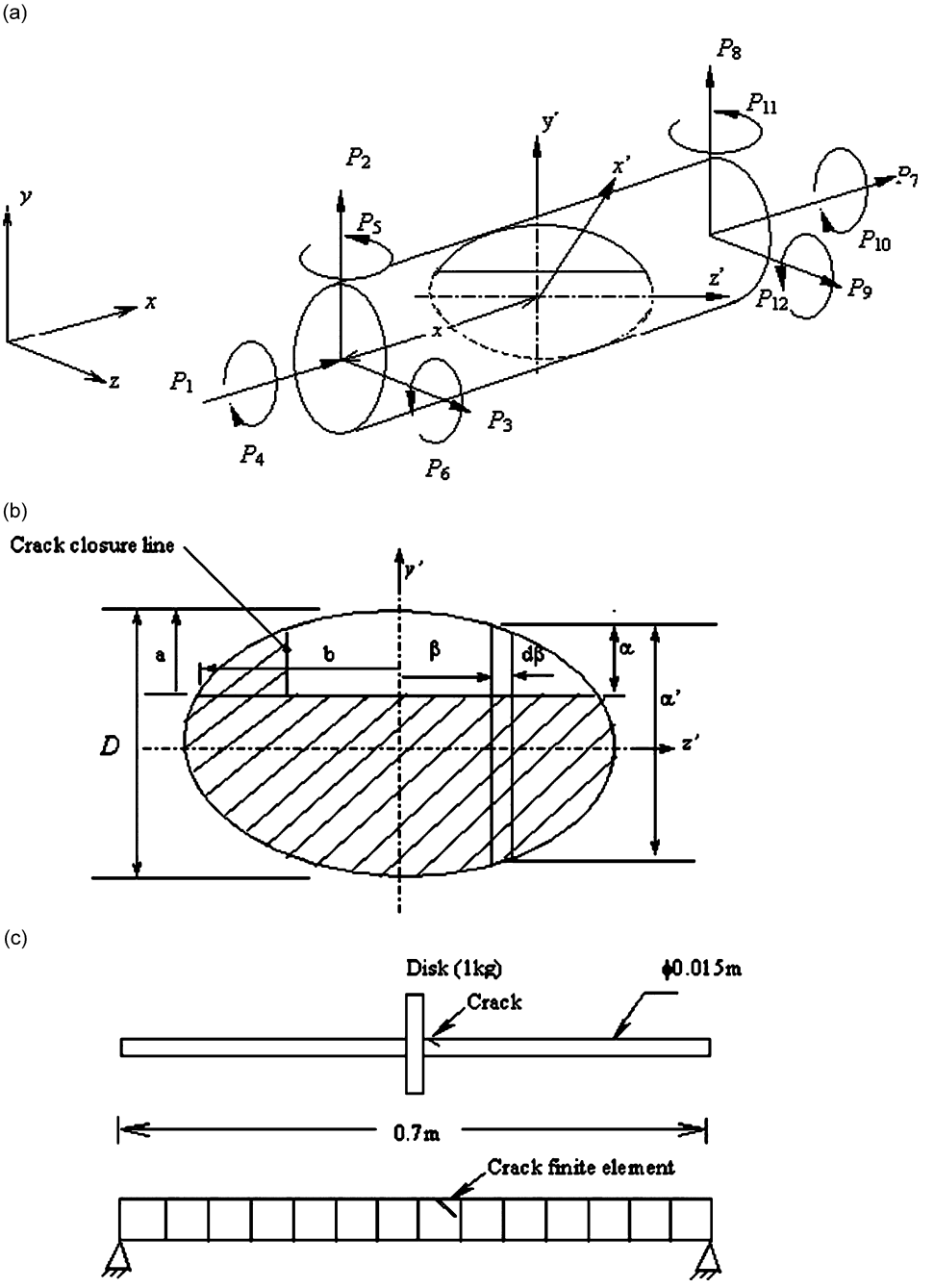

Fig. 1. Shaft finite element: (a) The element showing forces acting and coordinate system, (b) crack cross-section, (c) a simple rotor and its finite element model.

The flexibility matrix of the crack element is first derived. Let u_i and P_i are displacement and force, respectively, along ith coordinate. The flexibility coefficients are expressed as

$$g_{ij} = \frac{\partial}{\partial P_j}(u_i) = \frac{\partial^2}{\partial P_i \partial P_j}(U^o + U^c). \tag{1}$$

Here, U^o, strain energy of the uncracked shaft element; U^c, strain energy due to crack.

Considering the action of axial forces, torsion and bending moments and also accounting for shearing action at the cross-section of the crack the elastic strain energy of the element can be written as

$$U^o = \tfrac{1}{2}\int \left[\frac{\alpha_s V_1^2}{GA} + \frac{\alpha_s V_2^2}{GA} + \frac{M_1^2}{EI} + \frac{M_2^2}{EI} + \frac{T^2}{GI_o} + \frac{F^2}{AE}\right] \mathrm{d}x, \tag{2}$$

where, V_1, V_2 are the shear forces, M_1, M_2 the bending moments, T the torsional moment, F the axial force acting at the crack cross-section, G the modulus of rigidity, E the Young's Modulus, I the area moment of inertia of the cross-section, I_o the polar moment of inertia of the cross-section and α_s the shear coefficient.

Based on nodal forces acting on the FE, Eq. (2) can be written as

$$U^o = \tfrac{1}{2}\left[\frac{P_1^2 l}{AE} + \frac{\alpha_s P_2^2 l}{GA} + \frac{P_2^2 l^3}{3EI} + \frac{\alpha_s P_3^2 l}{GA} + \frac{P_3^2 l^3}{3EI} + \frac{P_4^2 l}{GI_o} + \frac{P_5^2 l}{EI} + \frac{P_6^2 l}{EI} - \frac{P_2 P_6 l^2}{EI} + \frac{P_3 P_5 l^2}{EI}\right]. \tag{3}$$

The additional strain energy due to the presence of crack is expressed as follows:

$$U^c = \frac{1}{E'}\iint_A \left[\left(\sum_{i=1}^{6} K_i^{\mathrm{I}}\right)^2 + \left(\sum_{i=1}^{6} K_i^{\mathrm{II}}\right)^2 + m_s\left(\sum_{i=1}^{6} K_i^{\mathrm{III}}\right)^2\right] \mathrm{d}A. \tag{4}$$

Here, $E' = E/(1-\upsilon)$ and $m_s = 1+\upsilon$; υ is Poisson's ratio. K_i^{I}, K_i^{II} and K_i^{III} represent SIF corresponding to opening, sliding and tearing mode of crack displacement, respectively ($i = 1$–6).

The SIFs are derived as follows. The forces P_1–P_{12} at the nodes act in a coordinate system x–y–z aligned along the shaft axis. The stresses due to these forces are resolved in another coordinate system aligned with the slant crack ($x' - y' - z'$) as shown in Fig. 1a, which, compared to transverse crack, leads to more number of stress components responsible for the opening and tearing mode of crack displacement. For example, stress due to shear force P_3 does not contribute to the opening mode in case of transverse crack whereas in slant crack case, its component σ_3^θ in the coordinate system $x' - y' - z'$ leads to opening mode of crack displacement (Fig. 2b). Similarly, axial force P_1 leads to shear stress τ_1^θ causing tearing mode for slant crack, in addition to opening mode due to normal component of σ_1^θ (Fig. 2c).

SIF for Mode 1(*opening mode*):

$$K_1^I = \frac{P_1}{\pi R^2}\sin^2\theta\sqrt{\pi\alpha}\,F_1, \tag{5}$$

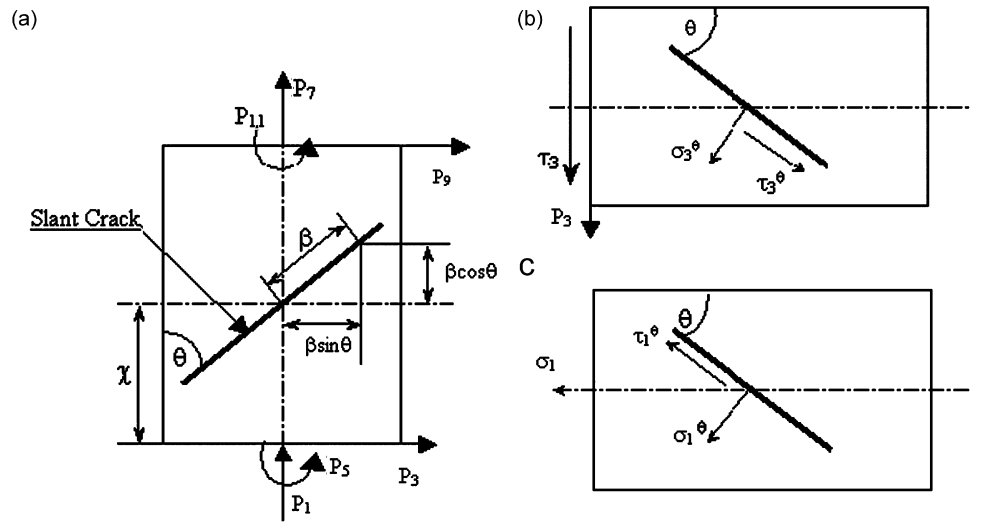

Fig. 2. Stress components on the slant crack: (a) Top view of the shaft element with slant crack showing position of the crack relative to shaft axis, (b) stress components due to shear stress τ_3, (c) stress components resulting from normal stress σ_1 due to axial force P_1.

where α is the depth of crack at any distance β from the centre along the crack edge (i.e., axis z' in Fig. 1b) and α' the total height of the strip of width $d\beta$ (Fig. 1b):

$$K_3^I = \frac{kP_3}{\pi R^2} \sin 2\theta \sqrt{\pi\alpha} F_1, \tag{6}$$

$$K_4^I = \frac{2P_4}{\pi R^4} \sqrt{R^2 - \beta^2 \sin^2\theta} \sin 2\theta \sqrt{\pi\alpha} F_2, \tag{7}$$

$$K_5^I = \frac{4(P_5 + P_3(\chi + \beta\cos\theta)}{\pi R^4} \beta \sin^3\theta \sqrt{\pi\alpha} F_1, \tag{8}$$

$$K_6^I = \frac{4(P_2(\chi + \beta\cos\theta) - P_6)}{\pi R^4} \sqrt{R^2 - \beta^2 \sin^2\theta} \sin^2\theta \sqrt{\pi\alpha} F_2, \tag{9}$$

$$K_2^I = 0. \tag{10}$$

SIF for Mode II (*sliding mode*):

$$K_2^{II} = \frac{kP_2}{\pi R^2} \sin\theta \sqrt{\pi\alpha} F_{II}, \tag{11}$$

$$K_4^{II} = \frac{2P_4}{\pi R^4} \beta \sin^2\theta \sqrt{\pi\alpha} F_{II}, \tag{12}$$

$$K_1^{II}, K_2^{II}, K_5^{II}, K_6^{II} = 0. \tag{13}$$

SIF for Mode III (*tearing mode*):

$$K_1^{III} = \left(\frac{P_1}{\pi R^2} \sin\theta\cos\theta\right) \sqrt{\pi\alpha}\, F_{III}, \tag{14}$$

$$K_3^{III} = \frac{kP_3}{\pi R^2} \cos 2\theta \sqrt{\pi\alpha} F_{III}, \tag{15}$$

$$K_4^{III} = \frac{2P_4 \sqrt{R^2 - \beta^2 \sin^2\theta}}{\pi R^4} \cos 2\theta \sqrt{\pi\alpha} F_{III}, \tag{16}$$

$$K_5^{III} = \frac{4(P_5 + P_3(\chi + \beta\cos\theta))}{\pi R^4} \beta \sin^2\theta \cos\theta \sqrt{\pi\alpha} F_{III}, \tag{17}$$

$$K_6^{III} = \frac{4(P_2(\chi + \beta\cos\theta) - P_6)}{\pi R^4} \sqrt{R^2 - \beta^2 \sin^2\theta} \sin\theta\cos\theta \sqrt{\pi\alpha} F_{III}, \tag{18}$$

where

$$F_1(\alpha/\alpha') = \sqrt{\frac{2\alpha'}{\pi\alpha} \tan\left(\frac{\pi\alpha}{2\alpha'}\right)} \frac{0.752 + 2.02(\alpha/\alpha') + 0.37\left[1 - \sin\left(\pi\alpha/2\alpha'\right)\right]^3}{\cos\left(\pi\alpha/2\alpha'\right)},$$

$$F_2(\alpha/\alpha') = \sqrt{\frac{2\alpha'}{\pi\alpha} \tan\left(\frac{\pi\alpha}{2\alpha'}\right)} \frac{0.923 + 0.199\left[1 - \sin\left(\pi\alpha/2\alpha'\right)\right]^4}{\cos\left(\pi\alpha/2\alpha'\right)},$$

$$F_{II}(\alpha/\alpha') = \frac{1.122 - 0.561(\alpha/\alpha') + 0.085(\alpha/\alpha')^2 + 0.18(\alpha/\alpha')^3}{\sqrt{(1 - (\alpha/\alpha'))}}$$

and

$$F_{\mathrm{III}}(\alpha/\alpha') = \sqrt{\frac{2\alpha'}{\pi\alpha}\tan\left(\frac{\pi\alpha}{2\alpha'}\right)}. \tag{19}$$

With the expressions of SIFs derived above, the additional strain energy due to crack given by Eq. (4) can be estimated. With $x_s = x + \beta\cos\theta$ and $R_b^2 = R^2 - \beta^2\sin^2\theta$, the expressions of flexibility for the slant crack shaft (given by Eq. (1)) can now be derived using strain energy Eqs. (3) and (4) as follows:

$$g_{11} = \frac{l}{AE} + \frac{1}{E'\pi R^4}\iint\left[\left(2\alpha\sin^4\theta F_{\mathrm{I}}^2 + 2m_s\alpha\sin^2\theta\cos^2\theta F_{\mathrm{III}}^2\right)\right]\mathrm{d}A,$$

$$g_{22} = \left(\frac{\alpha_s l}{GA} + \frac{l^3}{3EI}\right) + \frac{1}{E'\pi R^8}\iint\left[\begin{array}{l} 32x_s^2R_b^2\sin^4\theta\alpha F_{\mathrm{II}}^2 + 2R^4k^2\alpha\sin^2\theta F_{\mathrm{II}}^2 \\ +32m_sx_s^2R_b^2\alpha\sin^2\theta\cos^2\theta F_{\mathrm{III}}^2 \end{array}\right]\mathrm{d}A,$$

$$g_{33} = \left(\frac{\alpha_s l}{GA} + \frac{l^3}{3EI}\right) + \frac{1}{E'\pi R^8}\iint\left[\begin{array}{l} 32x_s^2\beta^2\alpha\left(\sin^6\theta F_{\mathrm{I}}^2 + m_s\sin^4\theta\cos^2\theta F_{\mathrm{III}}^2\right) + 16x_sk\beta\alpha R^2(\sin^3\theta\ \sin\ 2\theta F_{\mathrm{I}}^2 \\ +m_s\sin^2\theta\ \cos\ \theta\ \cos\ 2\theta F_{\mathrm{III}}^2 + 2k^2\alpha R^4(F_{\mathrm{I}}^2\sin^2 2\theta + m_s\cos^2 2\theta F_{\mathrm{III}}^2) \end{array}\right]\mathrm{d}A,$$

$$g_{44} = \frac{l}{GI_0} + \frac{1}{E'\pi R^8}\iint\left[\alpha\left(R_b^2\sin^2 2\theta F_2^2 + \beta^2\sin^4\theta F_{\mathrm{II}}^2 + m_sR_b^2\cos^2 2\theta F_{\mathrm{III}}^2\right)\right]\mathrm{d}A,$$

$$g_{55} = \frac{l}{EI} + \frac{1}{E'\pi R^8}\iint\left[\beta^2\alpha\left(\sin^6\theta F_{\mathrm{I}}^2 + m_s\sin^4\theta\cos^2\theta F_{\mathrm{III}}^2\right)\right]\mathrm{d}A,$$

$$g_{66} = \frac{l}{EI} + \frac{1}{E'\pi R^8}\iint\left[R_b^2\alpha\left(\sin^4\theta F_2^2 + m_s\sin^2\theta\cos^2\theta F_{\mathrm{III}}^2\right)\right]\mathrm{d}A,$$

$$g_{12} = \frac{8}{E'\pi R^6}\iint x_sR_b\alpha\left[\sin^4\theta F_1F_2 + m_s\sin^2\theta\cos^2\theta F_{\mathrm{III}}^2\right]\mathrm{d}A,$$

$$g_{13} = \frac{8}{E'\pi R^6}\iint x_s\beta\alpha\left[\sin^5\theta F_{\mathrm{I}}^2 + m_s\sin^3\theta\cos^2\theta F_{\mathrm{III}}^2\right]\mathrm{d}A + \frac{2}{E'\pi R^4}\iint k\alpha\left[\sin^2\theta\ \sin\ 2\theta F_{\mathrm{I}}^2 + m_s\ \sin\ \theta\ \cos\ \theta\ \cos\ 2\theta F_{\mathrm{III}}^2\right]\mathrm{d}A,$$

$$g_{14} = \frac{4}{E'\pi R^6}\iint\alpha R_b\left[\sin^2\theta\ \sin\ 2\theta F_1F_2 + m_s\ \sin\ \theta\ \cos\ \theta\ \cos\ 2\theta F_{\mathrm{III}}^2\right]\mathrm{d}A,$$

$$g_{15} = \frac{8}{E'\pi R^6}\iint\beta\alpha\left[\sin^5\theta F_{\mathrm{I}}^2 + m_s\sin^3\theta\cos^2\theta F_{\mathrm{III}}^2\right]\mathrm{d}A,$$

$$g_{16} = \frac{-8}{E'\pi R^6}\iint R_b\alpha\left[\sin^4\theta F_1F_2 + m_s\sin^2\theta\cos^2\theta F_{\mathrm{III}}^2\right]\mathrm{d}A,$$

$$g_{23} = \frac{32}{E'\pi R^6}\iint x_s^2R_b\beta\alpha\left[\left(\sin^5\theta F_1F_2 + m_s\sin^2\theta\cos^2\theta F_{\mathrm{III}}^2\right)\right]\mathrm{d}A + \frac{8}{E'\pi R^6}\iint x_sR_bk\alpha\left[\left(\sin^2\theta\ \sin\ 2\theta F_1F_2 + m_s\ \sin\ \theta\ \cos\ \theta\ \cos\ 2\theta F_{\mathrm{III}}^2\right)\right]\mathrm{d}A,$$

$$g_{24} = \frac{16}{E'\pi R^8}\iint x_sR_b^2\alpha\left[\left(\sin^2\theta\ \sin\ 2\theta F_2^2 + m_s\ \sin\ \theta\ \cos\ \theta\ \cos\ 2\theta F_{\mathrm{III}}^2\right)\right]\mathrm{d}A + \frac{4}{E'\pi R^6}\iint k\beta\alpha\sin^3\theta F_{\mathrm{II}}^2\,\mathrm{d}A,$$

$$g_{25} = \frac{32}{E'\pi R^8}\iint x_s R_b \beta\alpha\left[\left(\sin^5\theta F_1 F_2 + m_s \sin^3\theta\cos^2\theta F_{III}^2\right)\right] \mathrm{d}A,$$

$$g_{26} = -\frac{l^2}{2EI} - \frac{32}{E'\pi R^8}\iint x_s R_b^2 \alpha\left[\left(\sin^4\theta F_2^2 + m_s \sin^2\theta\cos^2\theta F_{III}^2\right)\right] \mathrm{d}A,$$

$$g_{34} = \frac{16}{E'\pi R^8}\iint x_s R_b \beta\alpha\left[\left(\sin^3\theta\ \sin\ 2\theta F_1 F_2 + m_s \sin^2\theta\ \cos\ \theta\ \cos\ 2\theta F_{III}^2\right)\right] \mathrm{d}A + \frac{4}{E'\pi R^6}\iint R_b k\alpha\left[\left(\sin^2 2\theta F_1 F_2 + m_s \cos^2 2\theta F_{III}^2\right)\right] \mathrm{d}A,$$

$$g_{35} = \frac{l^2}{2EI} + \frac{32}{E'\pi R^8}\iint x_s \beta^2\alpha\left[\left(\sin^6\theta F_1^2 + m_s \sin^4\theta\cos^2\theta F_{III}^2\right)\right] \mathrm{d}A + \frac{8}{E'\pi R^6}\iint k\beta\alpha\left[\left(\sin^3\theta\ \sin\ 2\theta F_1^2 + m_s \sin^2\theta\ \cos\ \theta F_{III}^2\right)\right] \mathrm{d}A,$$

$$g_{36} = \frac{-32}{E'\pi R^8}\iint x_s R_b \beta\alpha\left[\left(\sin^5\theta F_1 F_2 + m_s \sin^3\theta\cos^2\theta F_{III}^2\right)\right] \mathrm{d}A + \frac{-8}{E'\pi R^6}\iint k R_b \alpha\left[\left(\sin^2\theta\ \sin\ 2\theta F_1 F_2 + m_s\ \sin\ \theta\ \cos\ 2\theta F_{III}^2\right)\right] \mathrm{d}A,$$

$$g_{45} = \frac{16}{E'\pi R^8}\iint R_b \beta\alpha\left[\left(\sin^3\theta\ \sin\ 2\theta F_1 F_2 + m_s \sin^2\theta\ \cos\ 2\theta\ \cos\ \theta F_{III}^2\right)\right] \mathrm{d}A,$$

$$g_{46} = \frac{-16}{E'\pi R^8}\iint R_b^2 \alpha\left[\left(\sin^2\theta\ \sin\ 2\theta F_2^2 + m_s\ \sin\ \theta\ \cos\ 2\theta\ \cos\ \theta F_{III}^2\right)\right] \mathrm{d}A,$$

$$g_{56} = \frac{-32}{E'\pi R^8}\iint R_b \beta\alpha\left[\left(\sin^5\theta F_1 F_2 + m_s \sin^3\theta\cos^2\theta F_{III}^2\right)\right] \mathrm{d}A. \tag{20}$$

For $\theta = 90^\circ$, the slant crack represents the transverse crack and the above equations reduce to those derived in Ref. [10] for a transverse crack. For a general orientation of crack, the flexibility matrix of slant crack rotor (hereafter, slant crack would be referred to as crack with $\theta = 45^\circ$ unless otherwise specified) is given by

$$[G] = \begin{bmatrix} g_{11} & g_{12} & g_{13} & g_{14} & g_{15} & g_{16} \\ g_{21} & g_{22} & g_{23} & g_{24} & g_{25} & g_{26} \\ g_{31} & g_{32} & g_{33} & g_{34} & g_{35} & g_{36} \\ g_{41} & g_{42} & g_{43} & g_{44} & g_{45} & g_{46} \\ g_{51} & g_{52} & g_{53} & g_{54} & g_{55} & g_{56} \\ g_{61} & g_{62} & g_{63} & g_{64} & g_{65} & g_{66} \end{bmatrix}. \tag{21}$$

The above flexibility matrix is fully populated as against the flexibility matrix of the transverse crack, wherein some of the cross-coupled flexibilities do not exist (e.g., g_{45}, g_{46}, g_{14}). These cross-flexibility coefficients are important as they indicate the direct coupling of torsional mode ($i = 4$) with longitudinal ($i = 1$) and lateral modes ($i = 5$ and 6). For the transverse crack, the coupling between torsion and lateral modes comes through coupling of torsion and shear ($i = 4$ and 2, 3) due to crack and finally due to coupling of shear and bending in a Timoshenko beam. The above derivation for the slant crack demonstrates that the coupling between torsion and bending modes is direct and not only through shear deflection terms. It may be noted that in case of slant crack, the torsion, in addition to the usual shear mode SIF, also causes the opening mode and tearing mode SIFs that contribute to the deflections in bending and longitudinal modes. Later, it would be shown that this direct coupling leads to a stronger coupled vibration response in case of slant crack.

Due to the orientation of the slant crack, several force components introduce additional SIFs that do not apply for transverse crack. The derivation of flexibility coefficients presented here takes this fact into account.

The flexibility matrix is now used to find the stiffness matrix using the transformation matrix T considering static equilibrium of the FE:

$$\{q_{1-12}\}^{\mathrm{T}} = [T]\{q_{1-6}\}^{\mathrm{T}}, \tag{22}$$

where the transformation matrix is given by

$$[T]^{\mathrm{T}} = \begin{bmatrix} 1 & 0 & 0 & 0 & 0 & 0 & -1 & 0 & 0 & 0 & 0 & 0 \\ 0 & 1 & 0 & 0 & 0 & 0 & 0 & -1 & 0 & 0 & 0 & -l \\ 0 & 0 & 1 & 0 & 0 & 0 & 0 & 0 & -1 & 0 & -l & 0 \\ 0 & 0 & 0 & 1 & 0 & 0 & 0 & 0 & 0 & -1 & 0 & 0 \\ 0 & 0 & 0 & 0 & 1 & 0 & 0 & 0 & 0 & 0 & -1 & 0 \\ 0 & 0 & 0 & 0 & 0 & 1 & 0 & 0 & 0 & 0 & 0 & -1 \end{bmatrix}. \tag{23}$$

Thus, the stiffness matrix of the cracked element is written as

$$[K]^{c} = [T][G]^{-1}[T]^{\mathrm{T}}. \tag{24}$$

3. Stiffness variation due to crack breathing

For the evaluation of flexibility coefficients using Eq. (20), proper integration limits need to be considered to evaluate stiffness values. These limits depend on the amount of crack opening [5]. For fully open crack the limits can be taken from $-b$ to b, whereas for half-open half-closed crack these limits would be either from 0 to b or from $-b$ to 0 depending upon which half of the crack is open. To be able to study the flexibility variation with amount of crack opening, Darpe et al. [10] proposed a concept of crack closure line (CCL). The CCL is an imaginary line perpendicular to the crack edge. It separates the open and the closed parts of the crack as illustrated in Fig. 3, in which the right-half of the crack FE of Fig. 1a is shown in its different positions.

As the shaft element rotates, part of the slant crack opens and closes as shown in different angle of rotations in Fig. 3. The crack edge is divided into 50 points in the present case. Under gravity loading, the position of CCL keeps changing along the crack edge (say from 1 to 50) while opening from end of crack edge B to A ($\varphi = 0$–180°) and from 50 to 100 while closing from B to A i.e., for $\varphi = 180$–360°, as the rotor rotates clockwise. A continuous change of CCLP is indicative of breathing of the crack.

The variation of various stiffness coefficients evaluated using Eq. (24) as a function of CCL position is shown in Fig. 4. The stiffness coefficients are found for a crack FE of diameter $d = 0.015$ and length of $L = 0.05$ with a crack of depth $= 0.3$. The stiffness values are estimated for both slant ($\theta = 45^\circ$) and for transverse ($\theta = 90^\circ$) cracks to enable comparison. The figure shows that the slant crack is stiffer in longitudinal direction (k_{11}) and in bending (k_{66}). However, it is more flexible in shear (k_{22} and k_{33}) and has almost equal stiffness in torsion (k_{44}) compared to the transverse crack.

The sensitivity of the above stiffness values to crack depth is investigated and shown in Fig. 5. The variation of stiffness coefficients obtained from Eq. (24) with respect to CCL position is shown in the figure. As the crack gradually opens, all the stiffness values drop from those corresponding to uncracked shaft element till they become minimum at the fully open crack position (CCLP = 50). The stiffness variation is not quite noticeable for shallow depths of $\bar{a} = 0.1$ but is substantial for deeper crack ($\bar{a} > 0.2$). The drop in stiffness with crack depth is clearly nonlinear.

The comparative study of cross-coupled stiffness values for both slant and transverse crack FE is shown in Fig. 6. The cross-coupled stiffness coefficients play an important role in the coupled vibration response of the cracked rotor and from this point of view Fig. 6 provides important information. It may be noted that stiffness coefficient k_{16}, which is cross-coupled stiffness between longitudinal and lateral directions, is relatively weak for the slant crack compared to the transverse crack. Hence, the cross-coupling between lateral and longitudinal directions is weaker in case of slant crack. However, all other cross-coupled stiffness values are stronger for slant crack, particularly involving torsional displacement (e.g., k_{14}, k_{24}, k_{34}, k_{45} and k_{46}). In this paper, attention

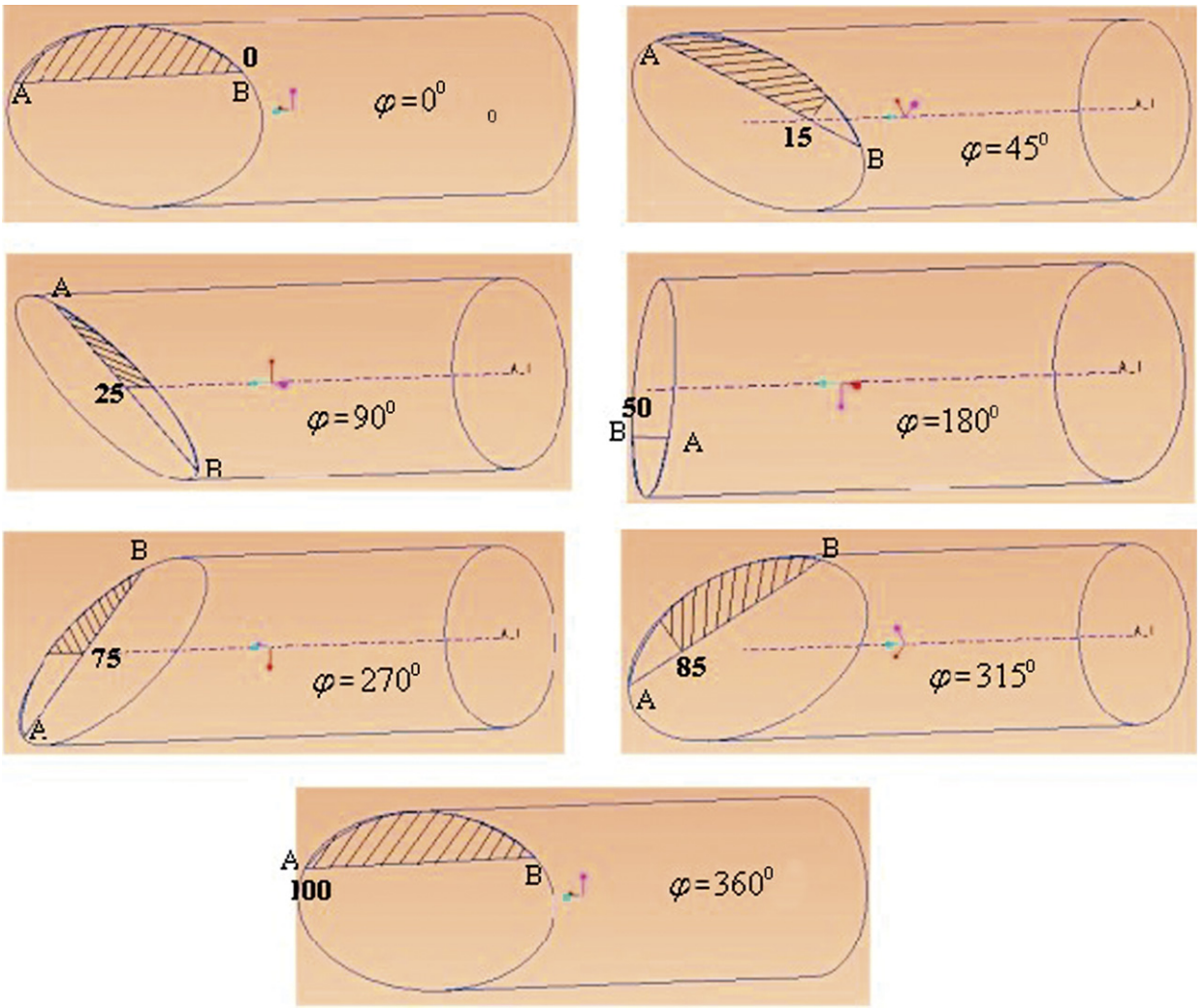

Fig. 3. Variation of crack closure line position with angular position of rotor.

is focussed in investigating the coupling of torsional vibrations with bending and longitudinal vibrations. In this light, the stronger coupling between torsional mode and other modes in case of slant crack as demonstrated in Fig. 6 provides strong basis for investigation of coupled torsional–bending–longitudinal vibrations.

The influence of angle of orientation of the slant crack with shaft axis (θ) on the stiffness values and variation of the stiffness values with CCLP is shown in Fig. 7. The figure shows that the drop in longitudinal stiffness (k_{11}) with amount of crack opening (indicated by CCLP) is maximum for transverse crack ($\theta = 90^\circ$) and the drop is minimum when angle is reduced from 90° towards zero. For shear stiffness (k_{22} and k_{33}) the stiffness drop is minimum for transverse crack. For the torsional stiffness (k_{44}), the largest stiffness drop occurs for $\theta = 30^\circ$. However, the stiffness drop first decreases from $\theta = 30^\circ$ to 60° and then increases from $\theta = 60^\circ$ to 90°. For lateral stiffness in plane parallel to the crack edge (k_{55}), the type of variation changes substantially due to the orientation of the crack.

4. Unbalance vibration response of rotor with slant crack

The calculation of stiffness of crack element and the vibration response estimation are interdependent. This is because the response is dependent on the stiffness values used in the equation of motion and stiffness

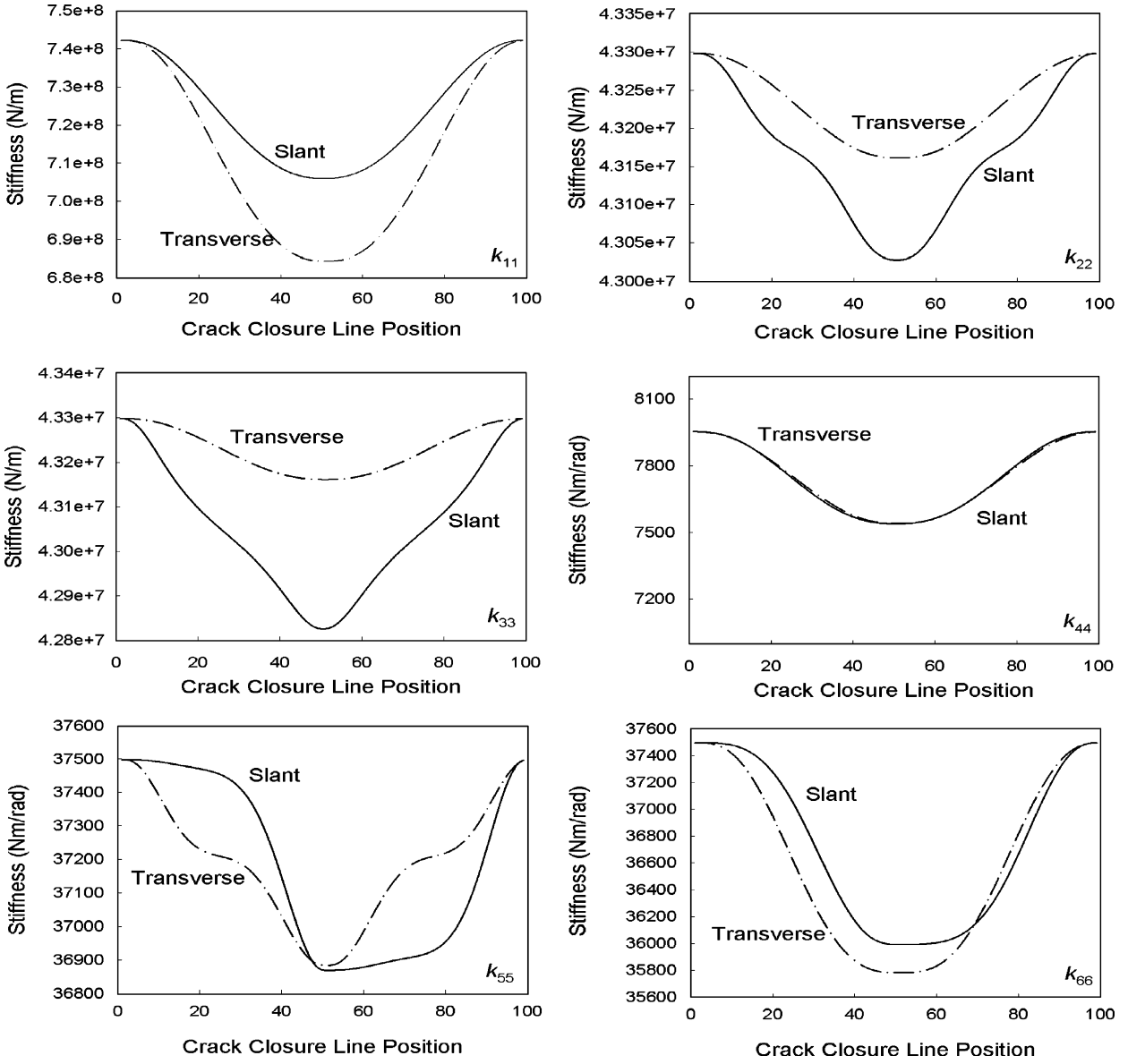

Fig. 4. Variation of direct stiffness coefficients with amount of crack opening.

values are estimated from the response using the sign of SIF values. The equation of motion in stationary coordinates is

$$[M]^s\{\ddot{q}\}^s + [C]^s\{\dot{q}\}^s + [K]^s\{q\}^s = \{f\}^s, \tag{25}$$

where $[M]^s$, $[C]^s$ and $[K]^s$ are global mass, damping and stiffness matrices for the rotor-bearing system in stationary coordinate system. Proportional damping matrix is assumed here with modal damping ratios of 0.005 and 0.01 in first two modes of the uncracked rotor system. The force vector $\{f\}^s$ contains gravity and unbalance excitation forces. When applied, torsional excitation terms also appear in the force vector. In the Newmark method of direct integration of equations of motion with a scheme similar to the one detailed in Ref. [10] is used with a sufficiently small time step of 1.5867e-5s. In the simulation, the mass and damping matrices are assumed constant and only stiffness matrix $[K]^s$ is constantly updated, after every degree of rotation to take care of the breathing behaviour. For this purpose, the nodal forces are used in Eqs. (5)–(18) to

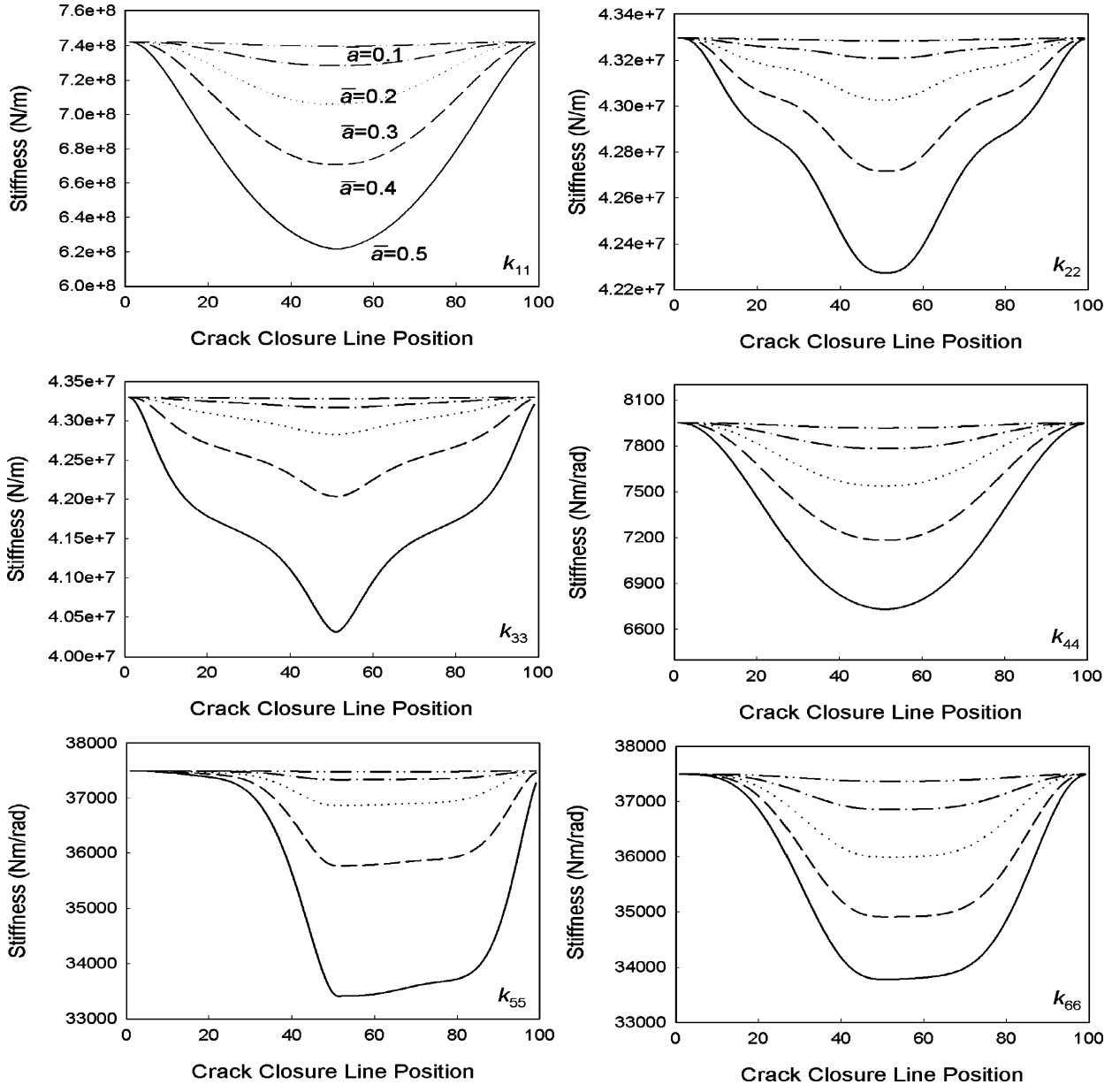

Fig. 5. Sensitivity of direct stiffness coefficients to crack depth for slant crack.

evaluate SIFs. Overall value of SIF (K^o) at 50 equally spaced points along the crack edge is evaluated using following relation:

$$K^0 = K_1^{\mathrm{I}} + K_3^{\mathrm{I}} + K_4^{\mathrm{I}} + K_5^{\mathrm{I}} + K_6^{\mathrm{I}}. \tag{26}$$

The position along the crack edge where SIF changes its sign is the crack closure line position (CCLP). Once the CCLP is ascertained, the flexibility matrix and crack element stiffness matrix is estimated. After transforming to stationary coordinate system, the element matrix is assembled in global stiffness matrix. The above-updated stiffness matrix along with an updated force vector corresponding to the new position of the rotor are then used to reevaluate the response of the rotor for the next one degree of rotation using Eq. (25). The response along with the new updated stiffness matrix is used to estimate new stiffness matrix and the process is repeated.

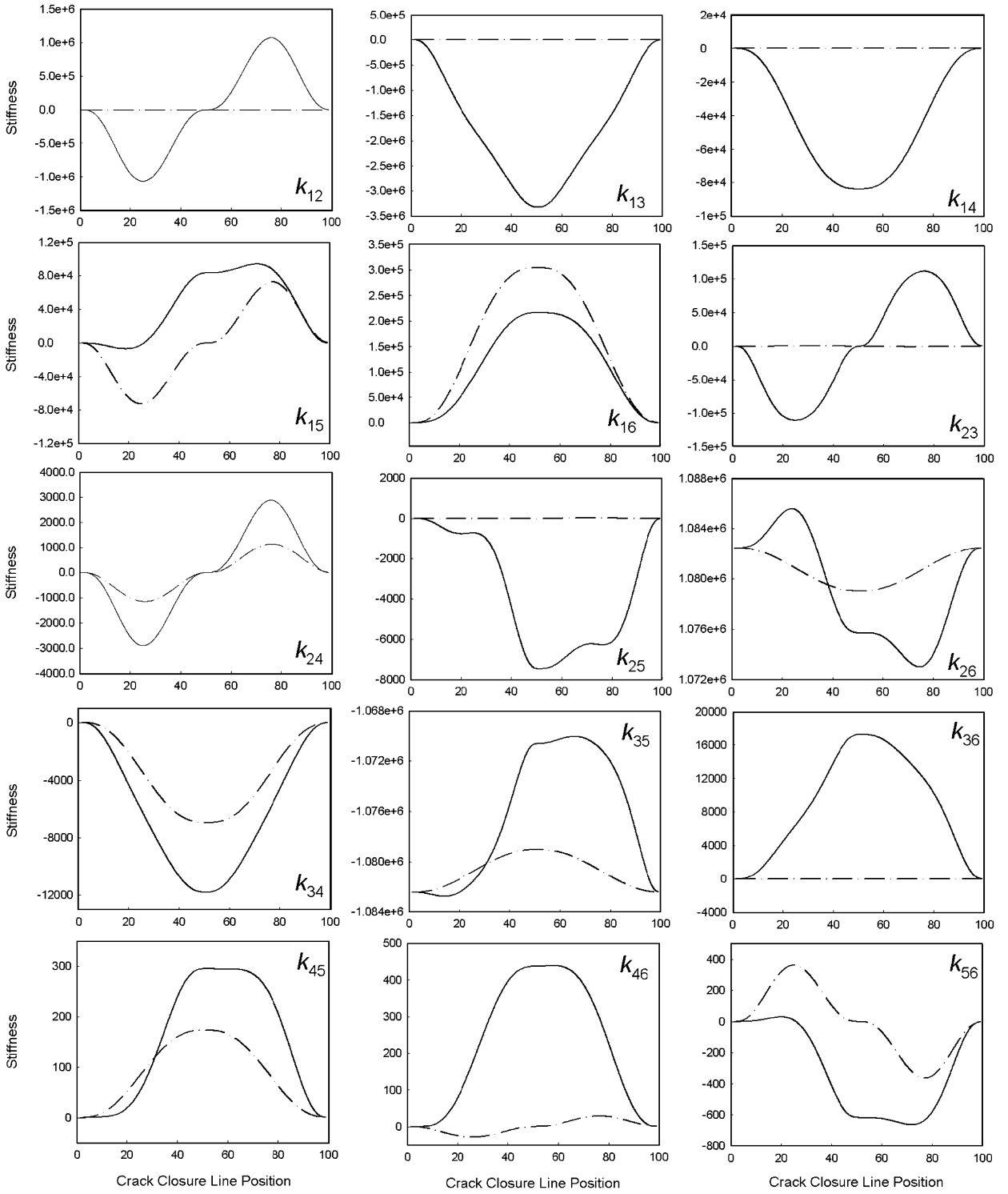

Fig. 6. Variation of cross-coupled stiffness values to amount of crack opening for slant (———) and transverse crack (— · —).

To study coupling of bending, longitudinal and torsional vibrations for slant crack, a simply supported rotor-bearing system with a single centrally situated disc of mass 1 kg is considered. A single slant crack is assumed just adjacent to the central disc. The total rotor span is divided into 14 elements of equal length

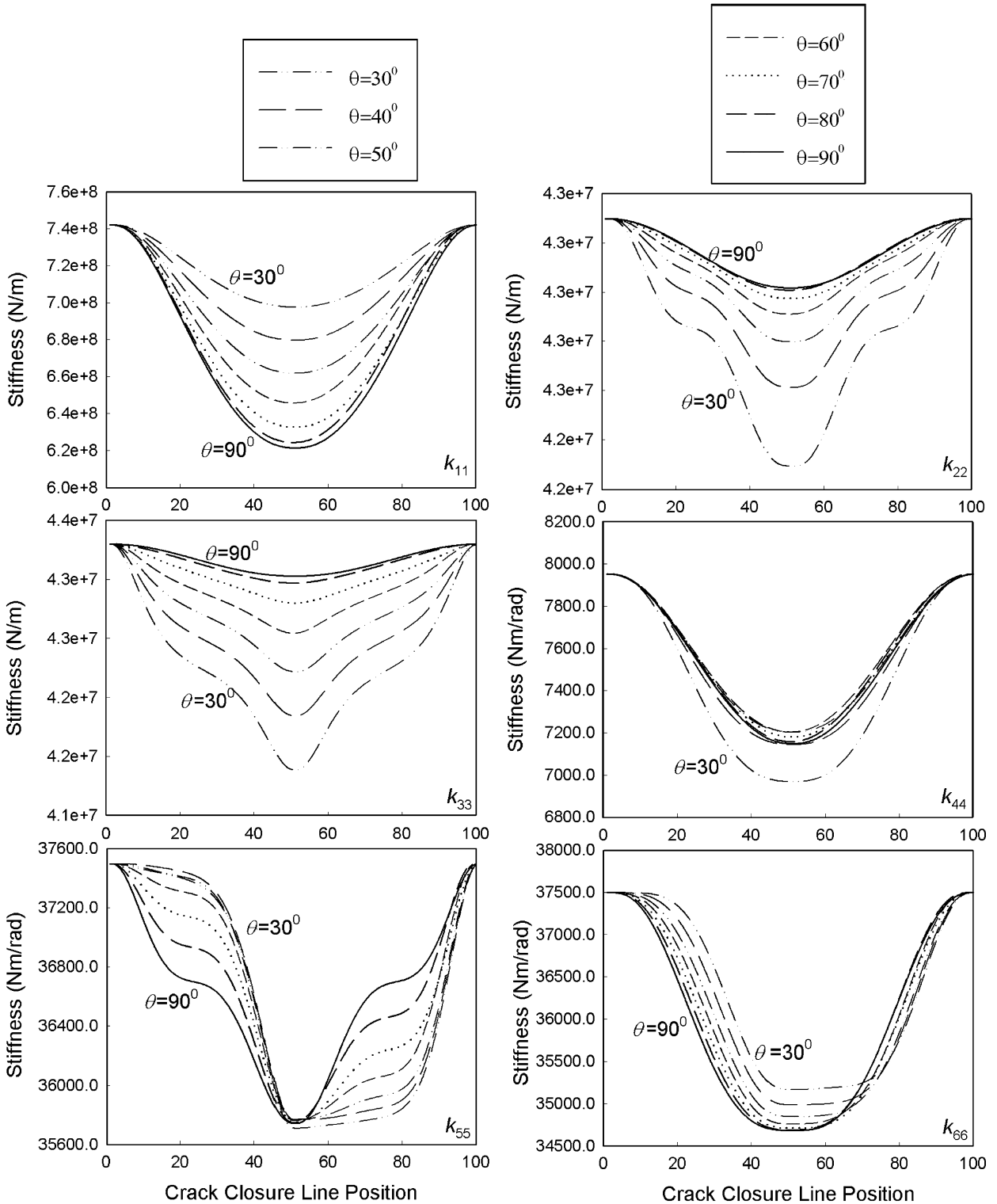

Fig. 7. Sensitivity of stiffness coefficients to angle of orientation of crack.

(Fig. 1c). A crack element that has stiffness properties as described in Section 2 is used to represent the crack. Rest of the rotor is modelled with Timoshenko beam elements with six degrees of freedom per node [17]. To start with, eignevalue analysis is carried out to ascertain the relative effect of transverse and slant crack on eigenvalues of the cracked rotor.

4.1. Eigenvalue analysis

The relevant natural frequencies obtained from the eigenvalue analysis of the rotor are summarised in Table 1 below. For comparison, natural frequencies for transverse crack are also mentioned.

It may be noted that the natural frequencies change marginally even for deeper cracks. It may also be noted that the frequency drop is always larger for transverse crack ($\theta = 90^\circ$) than for slant crack ($\theta = 45^\circ$) for bending and longitudinal mode, although in torsional mode and for deeper crack the drop is slightly more for slant crack. For shallower crack, the natural frequency drop for slant crack and transverse crack in torsional mode is same. The natural frequencies in the Table 1 are estimated based on fully open crack state and effect of breathing is not accounted for.

Compared with uncracked rotor the table clearly shows that even for deeper crack, the change in natural frequency in almost all modes of vibration is almost negligible. This drop is not measurable with reliability and hence the crack detection based on changes in the natural frequency is not practical. However, as elaborated in the later sections, the small stiffness changes for even the shallow depths of cracks are sufficient enough to generate easily detectable changes in the unbalance vibration response in time domain. These changes are highly sensitive to depth of crack and can be conveniently detected at lower depths. The changes are routinely represented in the frequency domain as the amplitudes of relevant frequency components lend themselves to be trended against time for crack depth monitoring. Hence, the time domain and frequency domain analysis of rotor vibration response are presented in the subsequent sections.

4.2. Vibration response of the rotor with slant crack

Initially, an unbalance response of the uncracked rotor is determined. The unbalance eccentricity of 1.6e-5m is assumed. The rotor rotates at 22 rad/s (3.5 Hz), which is approximately 1/10th of bending critical speed. Figs. 8a and c show the time domain response and Figs. 8b and d show the corresponding frequency spectra in the vertical and horizontal directions. The vibration spectra show an equal level of amplitude of rotational frequency of vibration in horizontal and vertical directions.

The unbalance response of a slant-crack rotor with crack depth ratio of $\bar{a} = 0.2$ rotating at 3.5 Hz is shown in Fig. 9. No torsional or axial excitation is applied to the system. Figs. 9a–d show how the lateral, longitudinal and torsional stiffness in rotor fixed coordinate system of the cracked rotor varies during a rotation. The lateral vibrations in both vertical and horizontal directions (Figs. 9i and j) contain 1st, 2nd and 3rd harmonic of rotational frequency. It may be noted that compared to the uncracked rotor the $1\times$ amplitude increases substantially for the cracked rotor (Fig. 8b and 9i) due to increased flexibility. Similarly, the longitudinal and torsional vibration spectra (Figs. 9k and l) show first two harmonics. The existence of rotational frequency and its higher harmonics in the torsional and longitudinal vibration spectrum without

Table 1
Comparison of natural frequencies (in Hz) for cracked and uncracked rotors ($\theta = 90^\circ$—transverse crack; $\theta = 45^\circ$—slant crack)

Mode	Uncracked	$\bar{a} = 0.2$		$\bar{a} = 0.4$	
		$\theta = 45^\circ$	$\theta = 90^\circ$	$\theta = 45^\circ$	$\theta = 90^\circ$
Bending (direction 5)	35.2	35.2	35.16	34.9	34.72
Bending (direction 6)	35.2	35.02	34.97	34.3	34
Torsional	125.8	125.6	125.6	124.7	124.8
Longitudinal	1248.1	1246.5	1245.6	1233	1220.9

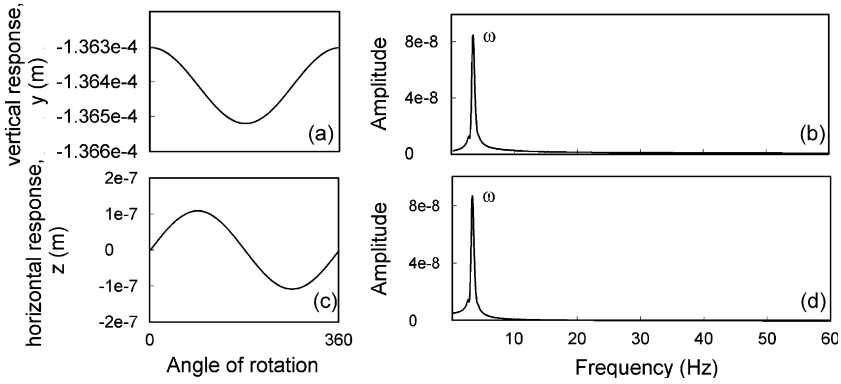

Fig. 8. Unbalance response of an uncracked rotor without torsional excitation: (a, b) response in vertical direction, (c, d) in horizontal direction. $\omega = 3.5$ Hz.

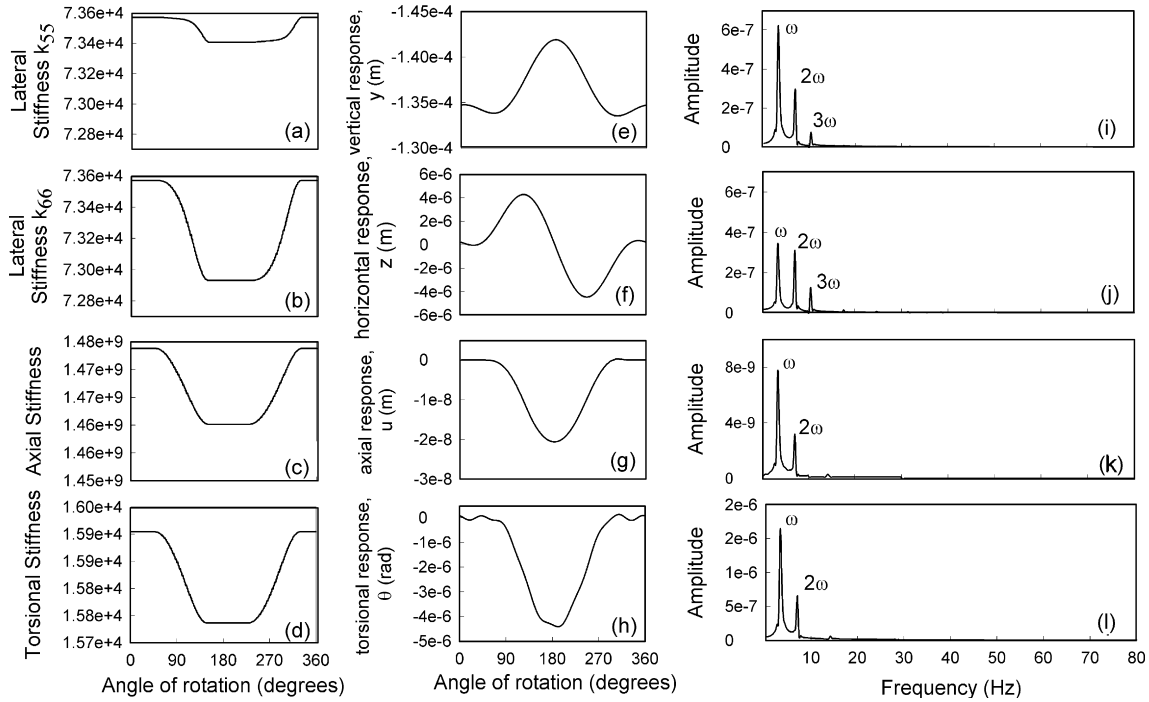

Fig. 9. Unbalance response of the slant-crack rotor ($\bar{a} = 0.2$) without torsional excitation ($\omega = 3.5$ Hz).

any explicit torsional or longitudinal excitation does indicate an existence of a prominent coupling mechanism between bending and torsion. The unbalance excitation in lateral direction generates torsional and longitudinal vibrations in the cracked rotor. The result shown in Fig. 9 thus indicates the coupling phenomenon between the bending and the torsional vibrations as well as between the bending and the longitudinal vibrations and is thus indicative of presence of crack.

In order to enhance the signals in all these spectra and to explore further the coupling phenomenon due to crack, a harmonic torsional excitation ($T\sin(\omega_e t)$) is applied at node 1 of the FE model. The torsional excitation is in addition to the unbalance excitation in the lateral direction at the disc location. The frequency of torsional excitation ω_e is tuned to the bending natural frequency of the system (ω_0). The purpose of such excitation is to check if this torsional excitation generates resonance in the bending vibration of the rotor as it would indicate a coupling mechanism between torsional and bending vibration in the rotor. Since in the

present rotor-bearing system no other coupling mechanism is considered, the response would eventually establish the presence of crack in the rotor. The speed of the rotor is 22 rad/s (3.5 Hz), which is 1/10th of the bending natural frequency of the uncracked rotor (35.2 Hz).

The time domain and frequency domain signals are shown in Fig. 10. Figs. 10a–d show variation in stiffness in lateral, longitudinal and torsional direction. Compared to Fig. 9 (without torsional excitation), marked difference in the stiffness variation is observed here. In Fig. 9, for unbalance excitation, the stiffness varied gradually and synchronously with rotation frequency, whereas in Fig. 10, for torsional excitation along with unbalance excitation, the stiffness changes synchronously with the torsional excitation frequency. The stiffness does not change gradually but fluctuate more abruptly; with stiffness values switching from fully closed state (e.g., indicated by $k_{66} = 73{,}570$ in Fig. 10b) to fully open state (e.g., indicated by $k_{66} = 72\,930$) almost instantly. This type of switching mode of crack breathing (used sometimes to simulate actual crack breathing) is described in the literature as "Hinge" model. The above simulation shows that in the case of slant-crack rotor under torsional harmonic excitation, the actual crack breathing is like that of the switching type ("Hinge" model) because of the orientation of the crack to the axis of the rotor and the type of excitation.

The time domain signals in horizontal and vertical directions (Figs. 10e and f) show beating phenomenon. The spectrum in vertical direction (Fig. 10i) shows rotational frequency and also the bending natural frequency that equals the torsional excitation frequency (ω_e). The frequency ω_e is flanked by side bands separated by rotational frequency (ω). The amplitude of bending natural frequency shows a large difference in the vertical and horizontal directions, whereas the amplitudes of sidebands around the excitation frequency ω_e are approximately the same in the two directions.

Owing to coupling of torsional and lateral vibrations the torsional excitation frequency appear in lateral vibration and the rotational frequency and its harmonics modulate the torsional excitation frequency. The interaction of the torsional excitation frequency (ω_e) with the rotational frequency (ω) and its harmonics ($m\omega$)

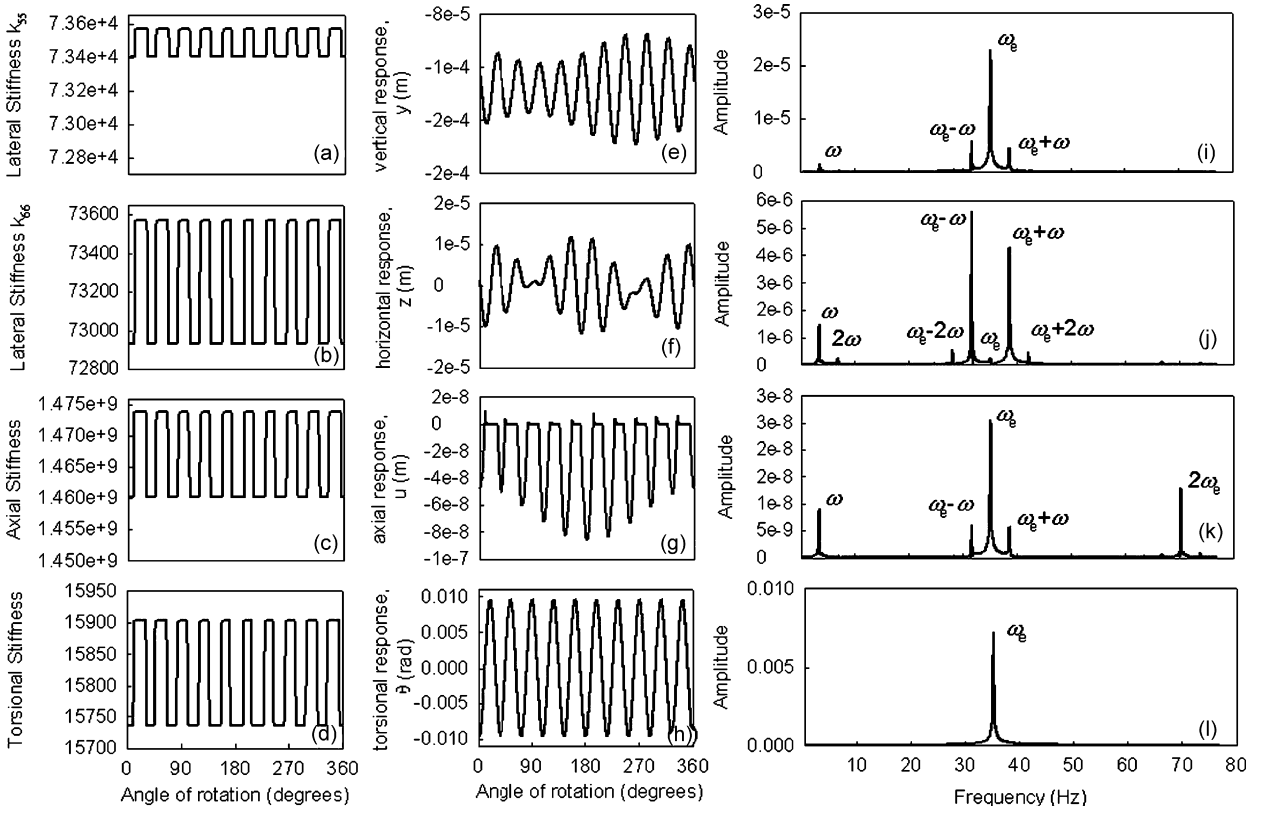

Fig. 10. Unbalance response of a slant-crack rotor ($\bar{a} = 0.2$) with torsional excitation; $\omega_e = \omega_0 = 35$ Hz and $\omega = 3.5$ Hz; $T = 10$ N m.

leads to the appearance of sum and difference frequencies ($\omega_e \pm m\omega$) around the torsional excitation frequency.

When compared with time domain signal of axial vibration without torsional excitation (Fig. 9(g), the application of torsional harmonic excitation brings about a distinctive change in the signal (Fig. 10(g). The presence of high frequency components is seen in the time domain signal and is confirmed in the frequency spectrum (Fig. 10k). The spectrum shows sidebands ($\omega_e \pm \omega$) around the torsional excitation frequency (ω_e). The strong presence of torsional excitation frequency (ω_e) indicates coupling between the torsional and longitudinal vibrations.

The time domain response of the longitudinal vibration (Fig. 10g) shows chopping of signal at the top and is prominently directed in one direction (−ve direction) about the zero deflection position. This abrupt chopping of the signal (at the same periodicity as the torsional excitation frequency ω_e) generates second harmonic component ($2\omega_e$) in longitudinal spectrum (Fig. 10k) although the torsional excitation is harmonic with frequency ω_e. This feature is related to the longitudinal stiffness variation pattern due to torsional excitation observed in Fig. 10c. The stiffness switches between fully closed to fully open state at torsional excitation frequency and the crack gets open and closed periodically as seen in the figure. As the crack closes, the response in longitudinal direction tends to drop to zero and when the crack opens, the response increases. The near exact matching of the timing of crack closure and response becoming zero corroborates this. It is worth mentioning that the similar observation is not noted in the lateral vibration response. The response in lateral vibration is due both to the unbalance excitation and due to the crack. In the longitudinal direction, there is no such additional excitation and the response is solely due to the crack.

The response of the slant-crack rotor with $\theta = 90^\circ$ is investigated under similar operating conditions. Slant crack at $\theta = 90^\circ$ means a transverse crack. Fig. 11 shows the stiffness variation and unbalance response of the transverse-crack rotor. The time domain response in lateral direction for the transverse crack as shown in Figs. 11e, i, f and j is qualitatively the same as that of the slant crack (Fig. 9) with approximately 20% larger

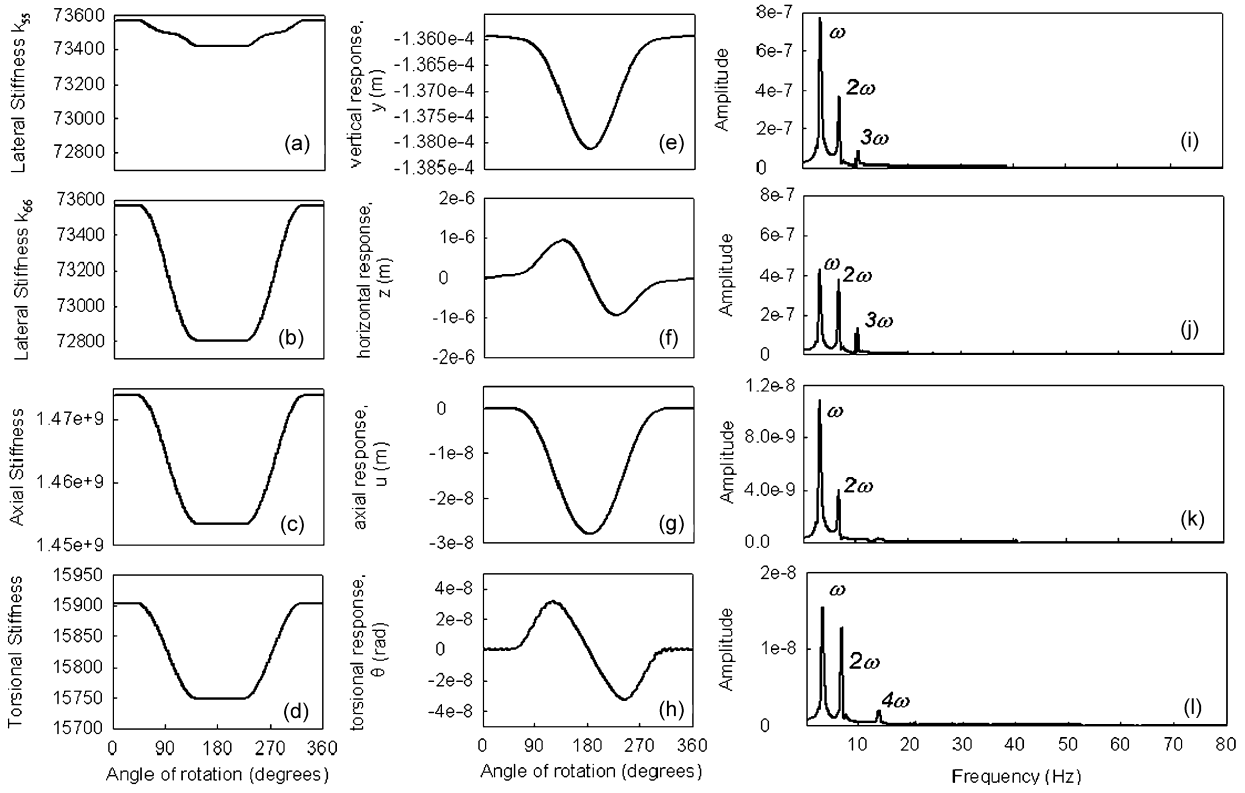

Fig. 11. Unbalance response of the transverse-crack rotor ($\bar{a} = 0.2$) without torsional excitation ($\omega = 3.5$ Hz).

amplitudes for the transverse crack. The amplitudes for longitudinal vibrations are also about 20% larger for transverse crack.

The amplitude of torsional vibration is much larger (about 100 times) for the case of slant crack (Fig. 9h) than the transverse crack (Fig. 11h). Torsional vibration frequency spectra also show important distinction; $1\times$ and $2\times$ frequency components have almost equal amplitudes in case of transverse crack, whereas, they have large difference in amplitude in case of slant crack. Apart from the lower amplitude of torsional vibration in case of transverse crack, the time domain response in torsion is also distinctly different in the two types of crack. The torsional deflection is much more asymmetric about the mean deflection of zero amplitude for slant crack (Fig. 9h) whereas the torsional deflection is more or less symmetric in case of transverse crack (Fig. 11h).

When the torsional excitation is applied to transverse crack rotor, the stiffness variation (Figs. 12a–d) is synchronous with rotational frequency and not with the torsional excitation frequency. Torsional excitation does not influence the opening and closing of transverse crack due to the (90°) orientation of the crack. Hence, the stiffness variation with and without torsional excitation is similar. However, because of the cross-coupled stiffness that do exist even for the transverse crack, lateral vibration response shows high frequency ripples (Figs. 12e and f). The presence of torsional excitation frequency and sidebands separated by rotation frequency (Figs. 12i and j) component is dominant in horizontal direction compared to the vertical direction.

When the response with torsional excitation is compared, the amplitude of torsional excitation frequency is more in horizontal direction than in vertical direction for transverse crack (Figs. 12i and j), whereas, for slant crack it is reverse(Figs. 10i and j). A very large difference exists in the amplitude of torsional excitation frequency in vertical direction between the slant crack (prominent presence) and transverse crack rotor (almost non-existent) (Fig. 10i and 12i). This frequency is having strong presence in the longitudinal spectrum for the slant crack and is absent in spectrum of transverse crack. Another important distinction is in presence of 2nd harmonic component of torsional excitation frequency in the longitudinal spectrum for slant crack.

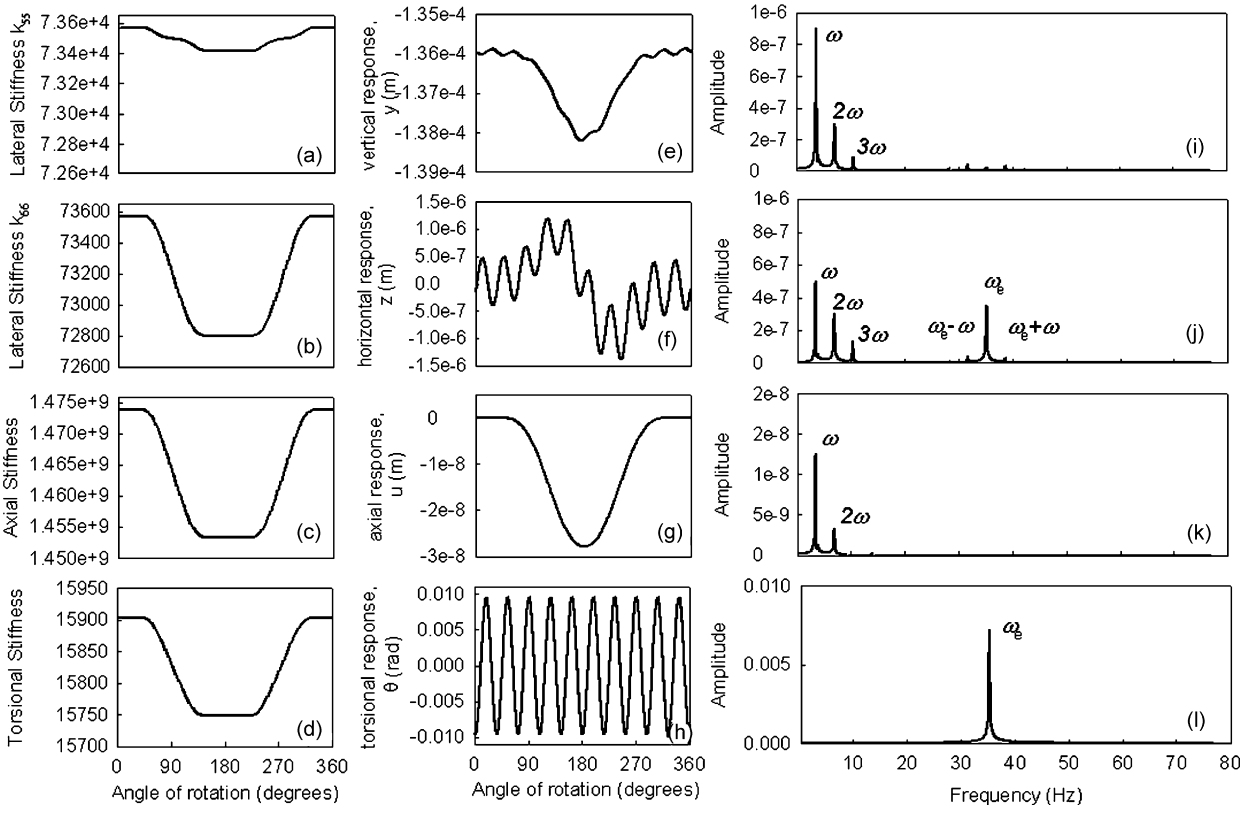

Fig. 12. Unbalance response of the transverse-crack rotor ($\bar{a} = 0.2$) with torsional excitation; $\omega_e = \omega_0 = 35\,\text{Hz}$ and $\omega = 3.5\,\text{Hz}$; $T = 10\,\text{N m}$.

The comparative study of the response features of slant and transverse crack discussed above gives enough information about the possible diagnostic strategy for detection and distinguishing the type of crack in a rotor. This is made possible due to the use of frequency domain analysis of the time domain vibration response of the rotor. The frequency domain representation reveals the exact frequency content and it was possible to correlate these frequencies with the two types of cracks.

4.3. Sensitivity analysis

The sensitivity of crack detection parameters (amplitudes of ω_e and $\omega_e \pm m\omega$ in lateral vibration spectra) to the depth of crack is very important and is shown in Fig. 13. As it is clearly observed, for both transverse and slant crack, the amplitude of torsional excitation frequency (ω_e) in bending vibration spectra increases with depth of crack. In horizontal direction, the torsional excitation frequency (ω_e) in case of transverse case is larger than in the vertical direction (Figs. 13a and b), whereas for the slant crack reverse is true (Figs. 13c and d). While in case of transverse crack, amplitude of the torsional excitation frequency in bending vibration spectrum in horizontal direction is very sensitive for the shallower crack depths (<0.3) as seen from Fig. 13b; this amplitude is more sensitive in vertical direction in shallower crack depths in case of slant crack (Fig. 13c). In comparison, this detection parameter is not very sensitive in vertical direction for transverse crack and in horizontal direction for slant crack.

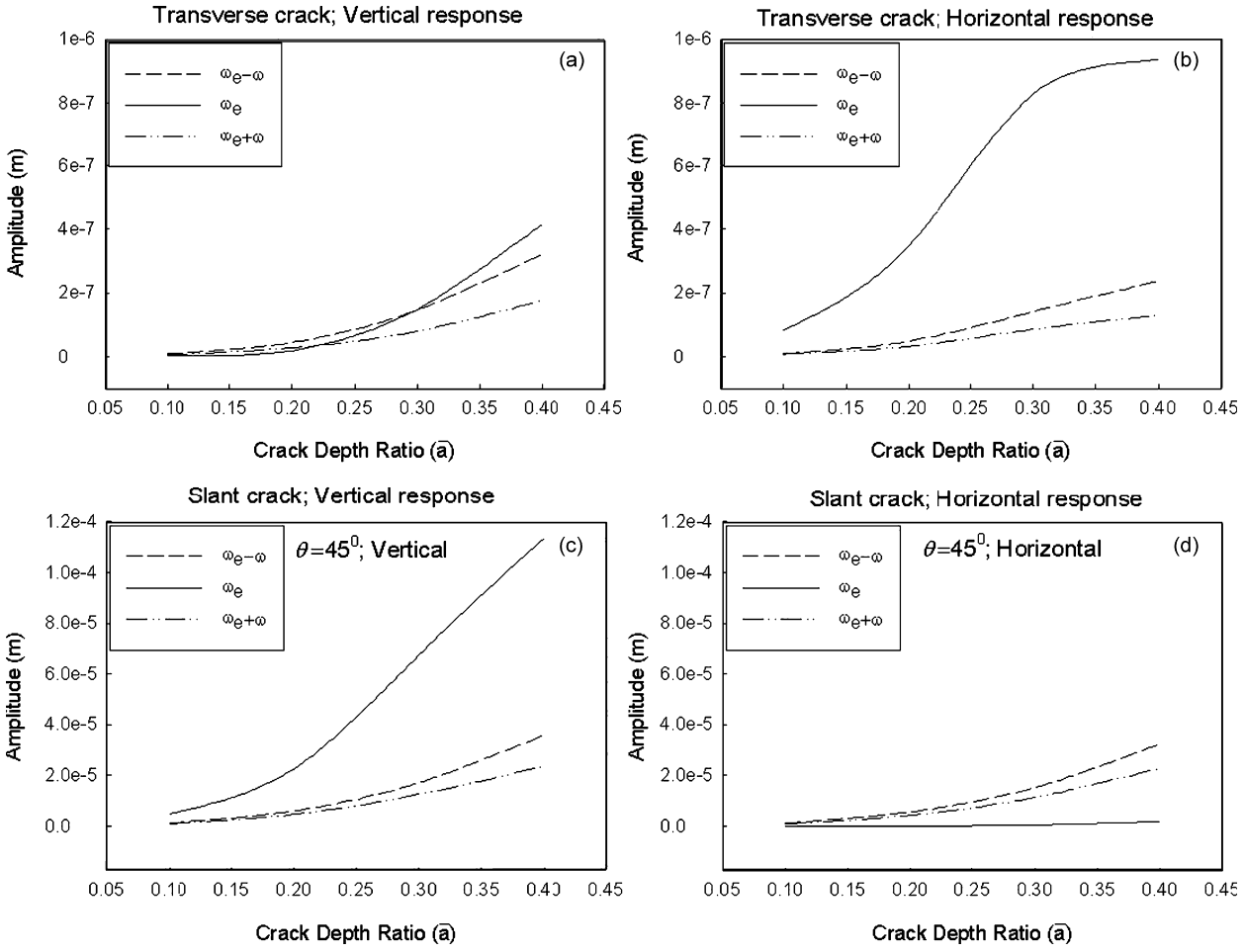

Fig. 13. Sensitivity of crack detection parameters to depth of crack.

Overall the sidebands ($\omega_e-\omega$ and $\omega_e+\omega$) around the torsional excitation frequency in the bending vibration spectrum are more or less of same magnitude as the torsional excitation frequency (ω_e) in vertical direction for transverse crack (Fig. 13a) whereas in horizontal direction the sidebands are comparatively of very small in amplitude relative to the amplitude of the torsional excitation frequency (Fig. 13b). Again the situation is exactly reverse in the case of slant crack as can be observed from Figs. 13c and d.

The amplitudes of various frequency components in the vibration response of the cracked rotor with slant and transverse crack show variation with crack depth with a distinguishing trend that can help in identifying the type of crack in a rotor-bearing system. The trend is direction specific (vertical/horizontal) and can be related to type of crack (slant/transverse). When the torsional excitation frequency in the lateral vibration response is trended over a period of time in both vertical and horizontal direction, then the continuous increase in the amplitude of this frequency component will indicate the presence of a fatigue crack. In addition, if the amplitude of the frequency in horizontal direction is stronger than in vertical direction, then the crack must be transverse crack, otherwise it must be a slant crack. Thus, the frequency component in the response and their directional nature helps us in detecting and identifying the type of crack in the rotor. These distinctive response features for identifying the type of crack (slant/transverse) in the rotor are the significant outcome of the present study.

The developed simulation procedure can be applicable to the turbomachinery rotors as the torsional excitation is always induced from blade excitation and also by electrical excitation from generator side. Sometimes transient torsional excitation can also be expected during load rejection and synchronisation. For crack detection, periodic measurements are also possible using additional torsional excitation and the present simulation gives ample evidence of detectable frequencies in the spectrum. The proposed detection method is important from practical application point of view in that the rotor is not stopped for the measurements allowing the diagnosis to be made in an online mode although preferably at lower speeds. In the earlier study in this area Papadopoulos and Dimarogonas [6] proved the existence of coupled torsional–bending vibrations through experimentation on a fixed–free non-rotating shaft with a transverse crack. The existence of crack has been detected based on the presence of bending natural frequencies in torsional spectrum and torsional natural frequencies in bending vibration spectrum while a sweep harmonic excitation was applied in either mode of vibration. However, they stressed that investigation in rotating shaft is required to propose a more realistic detection strategy. The improved study was required as rotation effect of rotor is expected to bring additional features for crack detection. In the results presented here, similar coupling has been proved. The only difference is that instead of torsional natural frequency, the torsional excitation frequency shows up in the bending vibration spectra and additional sidebands around the torsional frequency also appear. These frequencies are due to modulation by rotational frequency due to rotor rotation. These sidebands obviously did not appear in the spectra shown in Ref. [6] as they applied excitation to a stationary rotor. The present work in addition to supplementing similar results discussed in Ref. [10] also details an additional study on how to identify the type (slant/transverse) of crack in a rotor. A more systematic comparative study on response features of transverse and slant crack is presented.

A practical existence of coupling of vibrations in field rotors has been cited in Ref. [18], wherein a 300 MW steam turbine rotor in Greece showed coupled vibration response. In addition, Muszynska et al. [19] analytically and experimentally investigated torsional–lateral cross-coupled vibration response due to shaft anisotropy. They have experimentally shown the presence of subharmonic torsional resonance in lateral vibration at 1/8, 1/6, 1/4 and 1/2 critical speeds. Lateral split resonance in the bode plot of torsional vibrations and torsional resonance in the bode plot of lateral vibrations have been observed. Since the cracked rotor also introduces stiffness anisotropy, the validated results may apply for the cracked rotor. Theoretical results related to coupled lateral longitudinal vibrations has been validated in Ref. [9] by laboratory experimentation on transverse fatigue crack. However, a rigorous experimental investigation does not exist for slant crack in the past literature and can be attempted in future to validate coupling of lateral and torsional vibrations presented in this paper.

5. Conclusions

Coupled longitudinal–bending–torsional vibrations for slant crack rotor have been studied using FE model of the cracked rotor. The stiffness matrix of a beam element with slant crack based on additional strain energy

due to crack is derived. The stiffness matrix accounts for all the coupling mechanisms that exist in a rotor with slant crack. The FE with all the six degrees of freedom accounting for all the coupling mechanisms is used to explore coupled vibrations of a cracked rotating shaft. The coupled vibration response for both slant and transverse cracked rotor has been investigated for unbalance and torsional excitations with a response-dependent nonlinear breathing crack model.

The comparison of stiffness coefficients derived in this paper with those of transverse crack reveals that the slant crack exhibits a very strong cross-coupling of torsional and other modes of vibration (bending and longitudinal). This is revealed in larger torsional vibration to lateral unbalance excitation in the case of slant crack. The new stiffness matrix derived here shows a fully populated stiffness matrix for slant crack as additional SIFs are introduced due to orientation of the crack to shaft axis.

It is possible to detect whether the crack exists in a rotor based on the unbalance lateral vibration response to the additional torsional excitation. The torsional excitation frequency (and the sidebands around it) appears in lateral vibration spectra and are identified as potential crack detection parameters. A thorough comparison between the response of slant and transverse crack rotor has been carried out. Several distinctive features in their response are highlighted based on the coupled vibration response to torsional and unbalance excitation. Sensitivity analysis of the crack detection parameters (amplitudes of torsional excitation ferquency and sidebands in bending vibration spectra) has been carried out and it shows that these parameters are very sensitive to depth of crack. Comparing the amplitudes of torsional excitation frequency in vertical and horizontal directions in lateral vibration spectra, it is possible to detect the type of crack—transverse or slant. Similarly, steady-state time domain torsional vibration response and the frequency spectra of the cracked rotor subjected to unbalance excitation without torsional excitation, show distinctly different features for slant crack compared to the transverse crack that could be useful for identifying the type of crack. The results need to be validated by experimental investigations although inducing slant fatigue crack in rotors of experimental test rig is difficult if not impossible.

References

[1] J. Wauer, On the dynamics of cracked rotors—a literature survey, *Applied Mechanics Reviews* 43 (1990) 13–17.
[2] A.D. Dimarogonas, Vibration of cracked structures: a state of the art review, *Engineering Fracture Mechanics* 55 (1996) 831–857.
[3] I. Imam, S.H. Azzaro, R.J. Bankert, J. Scheibel, Development of an on-line rotor crack detection and monitoring system, *Journal of Vibration, Acoustics, Stress and Reliability in Design* 111 (1989) 241–250.
[4] R.A. Gasch, Survey of the dynamic behavior of a simple rotating shaft with a transverse crack, *Journal of Sound and Vibration* 160 (1993) 313–332.
[5] O.S. Jun, H.J. Eun, Y.Y. Earmme, C.W. Lee, Modeling and vibration analysis of a simple rotor with a breathing crack, *Journal of Sound and Vibration* 155 (1992) 273–290.
[6] C.A. Papadopoulos, A.D. Dimarogonas, Coupled vibration of cracked shafts, *Journal of Vibration and Acoustics* 114 (1992) 461–467.
[7] K.R. Collins, R.H. Plaut, J. Wauer, Detection of cracks in rotating Timoshenko shafts using axial impulses, *Journal of Vibration and Acoustics* 113 (1991) 74–78.
[8] A.K. Darpe, A. Chawla, K. Gupta, Analysis of the response of a cracked Jeffcott rotor to axial excitation, *Journal of Sound and Vibration* 249 (2002) 429–445.
[9] A.K. Darpe, K. Gupta, A. Chawla, Experimental investigations of the response of a cracked rotor to axial excitation, *Journal of Sound and Vibration* 260 (2003) 265–286.
[10] A.K. Darpe, K. Gupta, A. Chawla, Coupled bending, longitudinal and torsional vibrations of a cracked rotor, *Journal of Sound and Vibration* 269 (2004) 33–60.
[11] M. Ichimonji, S. Watanabe, The dynamics of a rotor system with a shaft having a slant crack, *JSME International Journal Series III* 31 (1988).
[12] M. Ichimonji, S. Watanabe, Y. Kazao, S. Nonaka, The dynamic of a rotor system with a slant crack under torsional vibration, *Proceedings of the International Mechanical Engineering Congress & Exposition*, Vol. 192, ASME, Illinois, 1994, pp. 81–89.
[13] A.S. Sekhar, P. Balaji Prasad, Dynamic analysis of a rotor system considering a slant crack in the shaft, *Journal of Sound and Vibration* 208 (1997) 457–474.
[14] C.A. Papadopoulos, A.D. Dimarogonas, Coupled longitudinal and bending vibrations of a rotating shaft with an open crack, *Journal of Sound and Vibration* 117 (1987) 81–93.
[15] S. Prabhakar, A.S. Sekhar, A.R. Mohanty, Transient lateral analysis of a slant-cracked rotor passing through its flexural critical speed, *Mechanisms and Machine Theory* 37 (2002) 1007–1020.
[17] H.D. Nelson, A finite rotating shaft element using Timoshenko beam theory, *Journal of Mechanical Design* 102 (1980) 793–803.

[18] C.A. Papadopoulos, A.D. Dimarogonas, Stability of cracked rotors in the coupled vibration mode, *Journal of Vibration, Acoustics, Stress and Reliability in Design* 110 (1988) 356–359.

[19] A. Muszynska, P. Goldman, D.E. Bently, Torsional/lateral vibration cross-coupled responses due to shaft anisotropy: a new tool in shaft crack detection, *Vibrations in Rotating Machineries—Proceedings of the International Conference, Institution of Mechanical Engineers*, 1992, pp. 257–262.